Journal of The Electrochemical Society, **150** (7) A985-A989 (2003)
0013-4651/2003/150(7)/A985/5/$7.00 © The Electrochemical Society, Inc.

Li^+ Storage Sites in Amorphous V_2O_5 Prepared by Precipitation Method

Tae Ahn Kim,[a] Jong Ho Kim,[a] Min Gyu Kim,[b] and Seung M. Oh[a,*,z]

[a]*School of Chemical Engineering and Research Center for Energy Conversion and Storage, Seoul National University, Seoul 151-744, Korea*
[b]*Pohang Accelerator Laboratory, Pohang University of Science and Technology, Pohang 790-784, Korea*

Amorphous vanadium oxide (a-V_2O_5) powders were prepared by acidifying aqueous NH_4VO_3 solution with concentrated nitric acid. Samples having a different degree of layer stacking and surface area were obtained either by changing the NH_4VO_3 concentration or by employing additional solvent exchange process. The pentane-exchanged precipitate gave the largest surface area (60 m^2 g^{-1}) after vacuum drying at 100°C for 24 h. This electrode material delivered an initial discharge capacity of 426 mAh g^{-1} in the voltage range of 1.5-4.0 V (*vs.* Li/Li^+), which amounts to 2.9 equiv Li^+ ions per mol of V_2O_5. X-ray absorption near-edge spectra (XANES) clearly showed a vanadium reduction down to V(III) when Li^+ ions were inserted at $Li^+/V_2O_5 > 2.0$. The Li^+ storage sites were analyzed by correlating the peak intensity in differential capacity plots to the surface area and degree of layer stacking, from which two different Li^+ storage sites were identified. The discharging capacity at 1.7 V was strongly correlated with the surface area of electrode material, suggesting that Li^+ ions are inserted into the amorphous region at this potential. The intensity of 2.5 V peak was, however, proportional to the peak intensity of (001) diffraction, illustrating that Li^+ ions are inserted into the quasi-ordered layer stacking region at this potential. The latter feature was further confirmed by X-ray diffraction analysis, whereby it was found that the interlayer spacing decreases most significantly near 2.5 V along with a sharp decrease in the (001) diffraction intensity.
 [DOI: 10.1149/1.1581260]

Manuscript submitted November 6, 2002; revised manuscript received January 20, 2003. Available electronically May 30, 2003.

Recently, sol-gel process has become widely used for preparing amorphous vanadium oxides via hydrolysis and condensation reaction of molecular precursors such as vanadium alkoxides.[1-6] Due to the difficulty in controlling the reaction rate in this process, however, a complexing agent such as acetyl acetone or acetic acid is commonly added. Another sol-gel method for vanadium oxides is the acidification of sodium metavanadate solution using ion-exchange resin.[7-12] A problem in this process is the contamination of Na^+ ions in the products and the difficulty in large-scale production. In these sol-gel processes, vanadium oxide xerogels are obtained upon drying the resulting gels under ambient condition or after solvent exchange.[13-15] The gels can also be converted to aerogels by supercritical drying.[16,17] Amorphous vanadium oxide xerogels or aerogels are known to have a higher Li^+ storage ability than the crystalline analogue when they are tested as the cathode material in Li secondary batteries. Four equivalents of lithium insertion per mole of V_2O_5 aerogel is frequently observed by chemical or electrochemical lithiation.[10] Moreover, some reports claimed even higher Li^+ storage capacity up to 5.8 equiv per mol of V_2O_5.[18] This high capacity has been ascribed in the literature to the amorphous structure and high surface area of these materials.[19,20] In this work, we utilized the rapid precipitation method to obtain amorphous vanadium oxide materials with an expectation that crystallization may be discouraged by a rapid precipitation so as to give a high surface area with a high degree of amorphicity. In brief, V_2O_5 precipitate was obtained by adding concentrated nitric acid into NH_4VO_3 aqueous solution at 100°C. The resulting precipitate was dried under ambient condition or dried after solvent exchange process. A reasonably high surface area was observed with a high degree of amorphous structure. This process seems much simpler than the conventional sol-gel ones in that neither the reaction rate control nor the use of ion exchange resin is needed.

When Li^+ ions are inserted into V_2O_5 lattice with $Li^+/V_2O_5 > 2.0$ according to the coupled electron/Li^+ insertion mechanism, the oxidation state of vanadium should be reduced to V(III). However, previous literature reported contradictory results on this issue. Some *in situ* X-ray absorption spectroscopy (XAS) studies suggested that vanadium oxidation state remains at V(IV) even for $Li^+/V_2O_5 > 2.0$.[21] To explain this electron-Li^+ imbalance, a surface cation-vacancy model has been proposed.[20,22-24] Recently, however, Mansour *et al.* provided the XAS result whereby vanadium oxidation state varies reversibly between V(V) and V(III) with electrochemical Li^+ insertion.[25]

The nature of Li^+ storage sites in a-V_2O_5 is not clearly identified in the literature. However, some Li^+ storage sites are undoubtedly associated with quasi-ordered interlayer region.[26-28] Intuitively, however, the amorphous portion in a-V_2O_5 should be an important Li^+ storage site because it is dominated by its amorphous nature and can be considered to be a more versatile host for Li^+ ions.

Three major goals were identified in this work: (*i*) to explore a new preparation method for amorphous V_2O_5 powder, (*ii*) to resolve the issue of electron-Li^+ imbalance, and (*iii*) to identify the Li^+ storage sites. To accomplish the first goal, a rapid precipitation of V_2O_5 and solvent exchange was performed. For the second goal, X-ray absorption near-edge spectra (XANES) were obtained by varying the Li^+/V_2O_5 ratio between 0 and 2.9, from which vanadium reduction down to V(III) was confirmed. For the last goal, the Li^+ storage capacity was correlated to the peak intensity of (001) diffraction in X-ray diffraction (XRD) patterns and also to the surface area of a-V_2O_5 materials.

Experimental

Materials.—The schematic procedure for the preparation of a-V_2O_5 powders is presented in Fig. 1. In detail, NH_4VO_3 was dissolved in hot distilled water. After a complete dissolution and removal of gaseous NH_3, concentrated nitric acid was added at 100°C. The reddish solution abruptly changed to brown precipitate. The resulting precipitate was collected by filtration, washed with water, and dried in a vacuum oven at 100°C for 24 h. For the solvent exchange, the precipitate was dispersed in organic solvent with stirring, and then the solvent was decanted. This process was repeated at least five times. Because pentane does not mix with water, pore water in the precipitate was first exchanged with acetone and then with pentane. The solvent-exchanged precipitate was collected by filtering and was dried in a vacuum oven at 100°C for 24 h.

Instrumentation.—XRD patterns were obtained with a rotating anode X-ray powder diffractometer (MacScience M18XHF-SRA)

* Electrochemical Society Active Member.
z E-mail: seungoh@plaza.snu.ac.kr

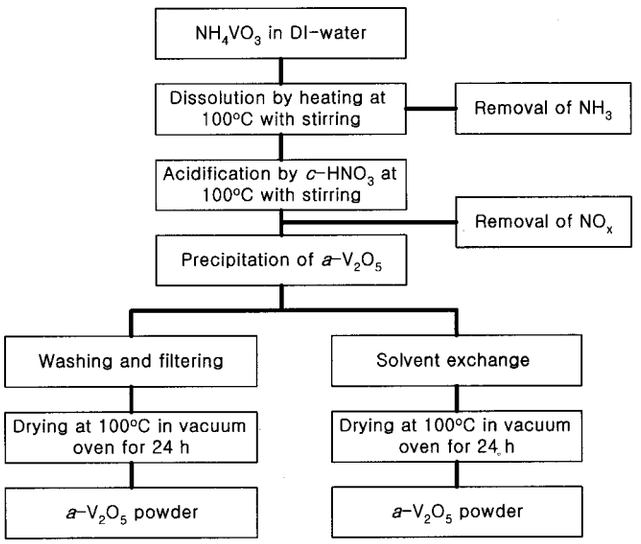

Figure 1. Synthetic procedure for a-V_2O_5 powders.

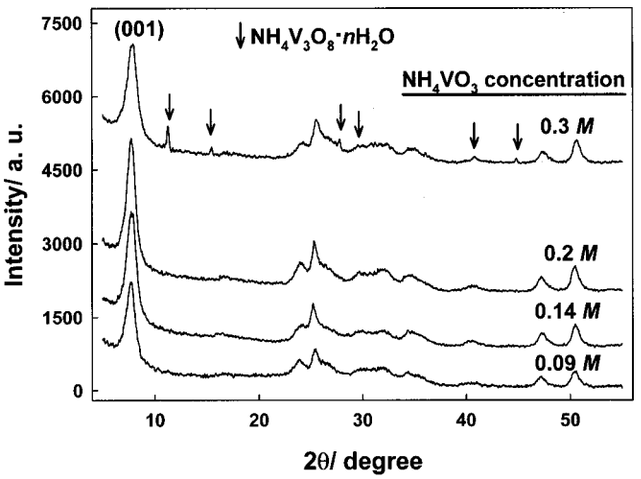

Figure 2. XRD patterns of a-V_2O_5 powders synthesized with different precursor (NH_4VO_3) concentration. The peak intensity of (001) diffraction steadily increased by increasing the precursor concentration until the impurity phase ($NH_4V_3O_8 \cdot nH_2O$) formed at >0.3 M.

using Cu Kα radiation at 50 kV and 100 mA. Silicon powder was added as an internal standard. Brunauer, Emmett, and Teller (BET) surface area was measured from the nitrogen adsorption isotherms. XANES were collected at the K-edge of vanadium (E_o = 5465.1 eV) in the transmission mode at the Pohang Accelerator Laboratory operating at 2.5 GeV with a current between 100 and 150 mA. A double-crystal Si(311) monochromator was used. The samples were sealed with Kapton film.

To prepare the composite cathodes, a-V_2O_5 powder was mixed with Ketjen black EC, and Teflon binder with a weight ratio of 70:20:10. The mixture was then dispersed in isopropyl alcohol and spread on a piece of stainless steel Exmet (long width dimension = 2 mm, short width dimension = 1 mm, apparent area = 1 cm^2), followed by a pressing and drying in vacuum at 120°C for 12 h. The used electrolyte was 1:1 mixture of ethylene carbonate (EC) and diethyl carbonate (DEC) containing 1.0 M $LiClO_4$ (Tomiyama Pure Chemical). The galvanostatic charge-discharge cycling was made in a three-electrode cell with a WBC-3000 battery cycler (Xeno Co.), where Li foil (Cyprus Co.) was used as the anode and reference electrode, respectively.

Results and Discussion

Preparation of a-V_2O_5 by precipitation method.—The preparation condition, surface area, and first discharge capacity are listed in Table I. The top five samples were prepared as a function of NH_4VO_3 concentration, whereas sample VO-3 and the bottom three samples were prepared by changing the solvent in the solvent exchange step while the NH_4VO_3 concentration was fixed at 0.2 M. Samples obtained without the solvent exchange process exhibited a surface area of $<10\ m^2\ g^{-1}$. However, surface area is enlarged by the solvent exchange process. Here, surface area became larger as the surface tension of the solvent used decreased. This feature is common in sol-gel processes where solvent-exchange or supercritical drying is involved. In normal drying, large capillary forces at the liquid-solid interface cause porous materials to shrink or crack when the pore water is removed by evaporation. When the pore water is replaced by solvents of a lower surface tension, the pore structure sustains with a limited collapse because a lesser surface tension is exerted across the pores. In this work, the pentane-exchanged precipitate gave rise to the largest surface area.

The XRD profiles of four samples are represented in Fig. 2. Generally, the XRD peaks are broad and weak, indicative of an amorphous nature of prepared samples. The most intense peak located at 8° is the (001) diffraction, which is related to the ribbon stacking along the *c* axis and thus the (001) peak intensity is assumed to be proportional to the fraction of quasi-ordered crystalline material in the samples. In Fig. 2, it is seen that the intensity of (001) peak gradually increases as the NH_4VO_3 concentration becomes higher, indicative of a gradual increase in the fraction of quasi-ordered region in the samples. For the sample synthesized with a high concentration (0.3 M), the electrochemically inactive impurity phase ($NH_4V_3O_8 \cdot nH_2O$) develops as shown in the top

Table I. Synthetic conditions for a-V_2O_5 powders and their surface area and first discharge capacity.

Sample	NH_4VO_3 Concn (M)	Solvent	Surface tension ($mN\ m^{-1}$)	Surface area ($m^2\ g^{-1}$)	First discharge capacity ($mAh\ g^{-1}$)
VO-1	0.09	Water	71.99	3.20	308
VO-2	0.14	Water	71.99	3.43	367
VO-3	0.20	Water	71.99	5.02	381
VO-4	0.26	Water	71.99	4.77	376
VO-5	0.30	Water	71.99	3.83	364
VO-6	0.20	Acetone + water (1:1 wt %)	40.63[a]	16.48	385
VO-7	0.20	Acetone	23.46	40.56	415
VO-8	0.20	Pentane	15.49	59.94	426

[a] This value was calculated from the method of Tamura *et al.*[29] Others from *CRC Handbook of Chemistry and Physics*, 81st ed.

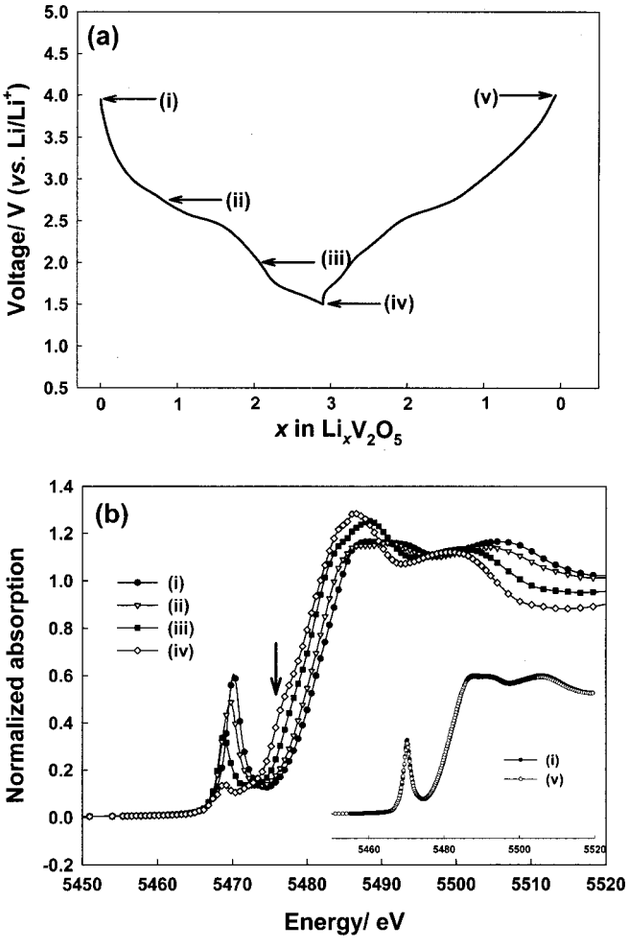

Figure 3. (a) Galvanostatic charge-discharge profiles traced with sample VO-8 at a current density of 30 mA g^{-1} and (b) vanadium K-edge XANES spectra of a-V_2O_5 electrode recorded with charge-discharge cycling. The voltages where the spectra were taken are indicated in (a). At the inset, the spectra obtained before and after the cycling are provided, where it is noted that two spectra are identical, indicative of a reversible reaction between a-V_2O_5 and Li^+ ions.

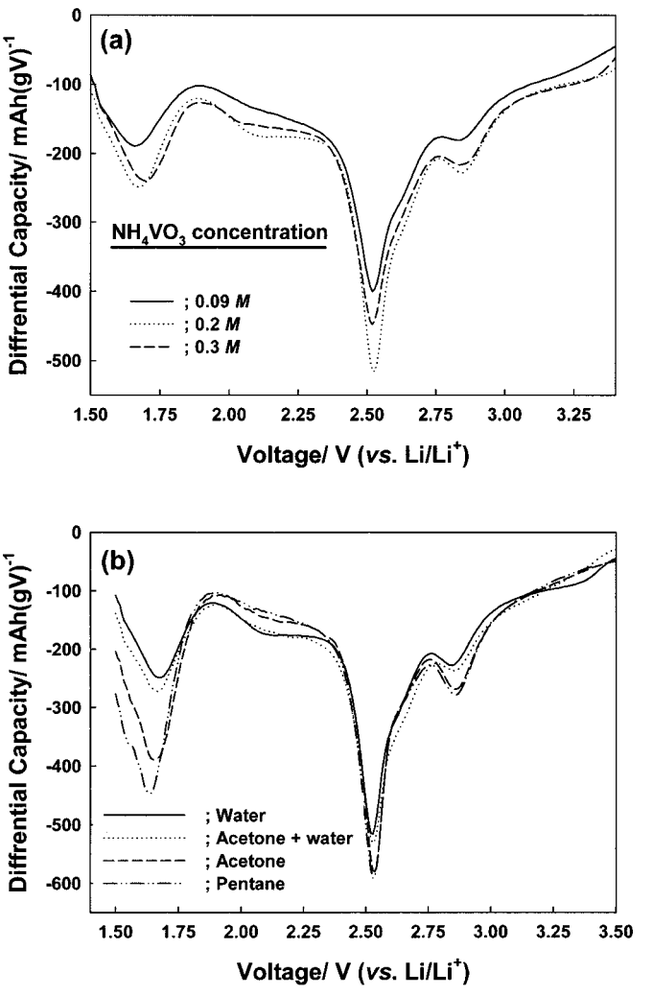

Figure 4. The differential discharging capacity plots (dQ/dV *vs.* V) that were obtained by differentiating the galvanostatic discharging profiles for the (a) samples prepared with different precursor concentration and (b) samples prepared by changing the solvent. Note that the peaks appearing at 1.7, 2.5, and 2.9 V differ in intensity for the samples.

profile. The sample prepared with 0.2 M NH_4VO_3 exhibits the highest (001) diffraction peak among the samples. All samples showed an interlayer spacing of 1.15 ± 0.01 nm within experimental error. The XRD patterns also showed other peaks that are related to the internal ribbon structure.[30] The layer spacing and XRD patterns are similar to those of a-V_2O_5 reported by others.[31,32]

The issue of electron-Li^+ imbalance in a-V_2O_5.—Figure 3a displays a galvanostatic charge-discharge profile obtained with sample VO-8. Li^+ insertion/extraction occurs over the entire voltage region of 1.5-4.0 V (*vs.* Li/Li^+), but there appears a plateau-like behavior at 2.9, 2.5, and 1.7 V. The specific discharge capacity of this electrode was 426 mAh g^{-1} at a current density of 30 mA g^{-1}. Assuming 100% coulombic efficiency, an insertion of 2.9 mol of Li^+ per mol of a-V_2O_5 is calculated. Figure 3b presents the XANES spectra of this sample taken as a function of lithium content. Upon lithiation, the X-ray edge energy for vanadium is gradually shifted toward the lower energy as a consequence of a vanadium reduction. A careful inspection on the spectrum for $Li^+/V_2O_5 = 2.9$ reveals that vanadium is reduced to V(III), which is confirmed by the emerging shoulder located by the arrow. This observation is identical to that reported by Mansour *et al.*[25] From this, it is likely that the coupled electron/Li^+ insertion prevails in this sample and vanadium is reduced to V(III). The intensity of pre-edge peak, related to the probability of dipole forbidden s → d electronic transition, steadily decreases with Li^+ insertion. The intensity of this peak is proportional to the deviation from octahedral symmetry of the vanadium sites and its decrease is likely related to the modifications of vanadium local environment that becomes more symmetric upon lithiation.[33,34] Curves in the inset, traced before and after the cycling, show that two spectra are identical to each other, manifesting themselves that Li^+ insertion/extraction process is reversible without severe deformation in the lattice structure and electronic states.

The nature of Li^+ storage sites in a-V_2O_5.—Figure 4 shows the differential capacity (dQ/dV *vs.* V) profiles that are derived from the galvanostatic discharging profiles (for example, that shown in Fig. 3a). The profiles obtained with a-V_2O_5 electrodes that were prepared with a variation in the NH_4VO_3 concentration are provided in Fig. 4a, whereas those profiles obtained with samples prepared with solvent exchange are in Fig. 4b. The plateau-like behavior in Fig. 3a appears as a peak at 2.9, 2.5, and 1.7 V in the profiles. It is apparent in both figures that the intensity of three peaks differs for the samples, indicative of a different population of Li^+ storage sites.

The peak intensity at 1.7 V in the differential capacity plots was normalized by that of sample VO-8, and then correlated to the

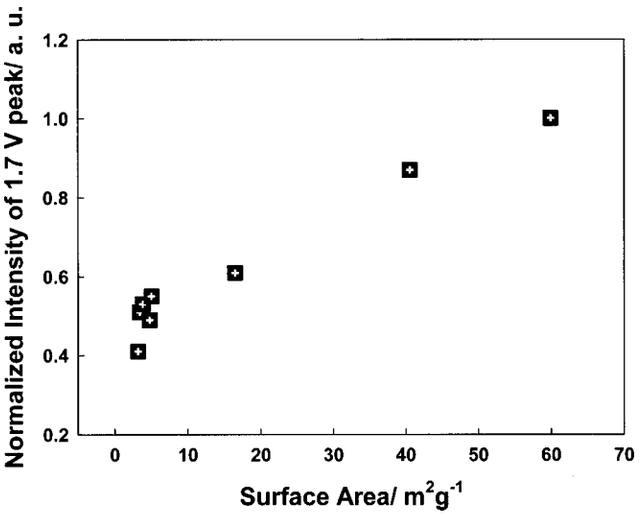

Figure 5. The correlation between the normalized peak intensity of 1.7 V in the differential capacity plots and the surface area of electrode materials. The normalization procedure is described in the text. Note a strong correlation between two parameters.

surface area of the samples (Fig. 5). Note that the peak height from the baseline was taken as the peak intensity due to the difficulty in deconvolution, thereby the intensity values carry a certain degree of uncertainty. Despite this, there appears a strong correlation between the peak intensity at 1.7 V and the surface area. Upon considering that the surface area is related with the population of amorphous region in the samples, it is likely that Li^+ ions are stored at the amorphous region at 1.7 V.

The (001) peak intensity in XRD patterns is a measure of the population of quasi-ordered layer stacking in the samples. In Fig. 6, the normalized peak intensity of (001) diffraction (Fig. 2) was correlated to the normalized peak intensity at 2.5 V. Here again, two parameters are well correlated to each other even if some data are scattered, illustrating that Li^+ ions are inserted into the ordered stacking layers at 2.5 V. To further confirm this feature, XRD study was made with a variation in the degree of charge/discharge. In

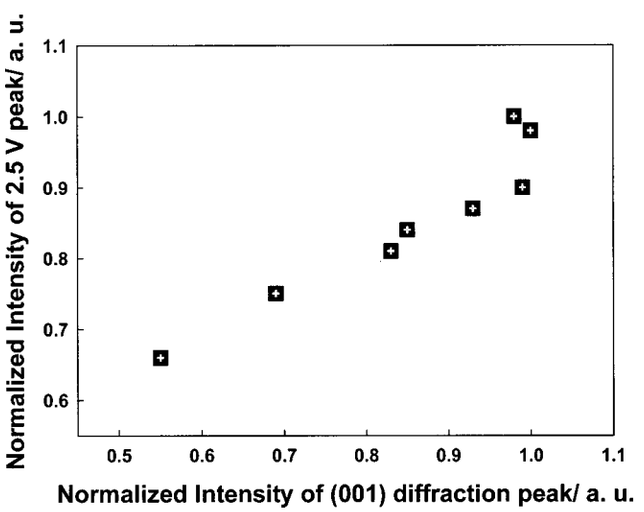

Figure 6. The correlation between the normalized peak intensity of 2.5 V in the differential capacity plots and the normalized peak intensity of (001) diffraction in XRD profiles. Note a strong correlation between two parameters.

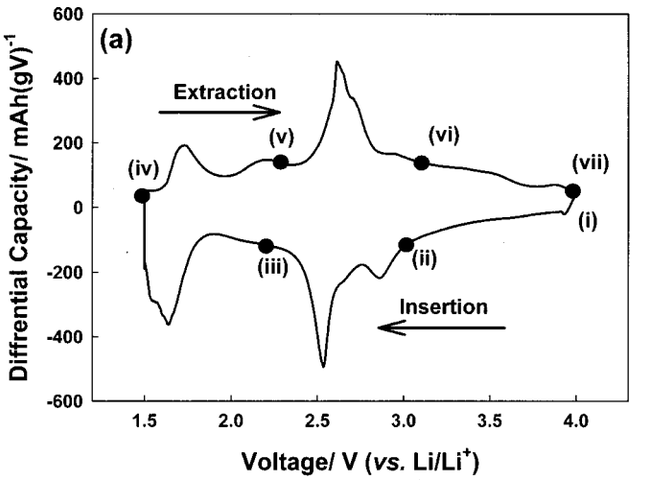

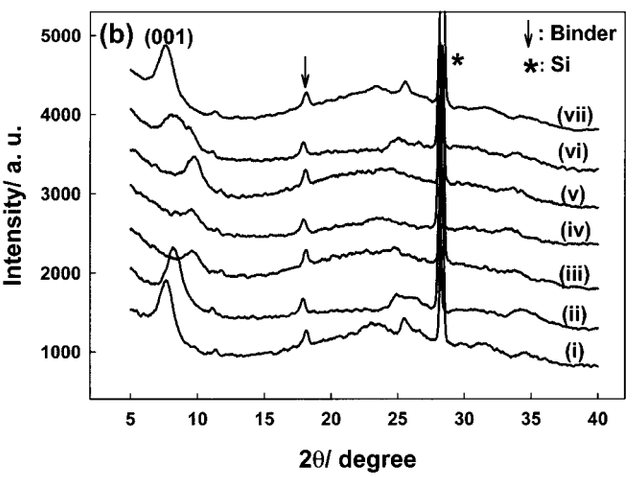

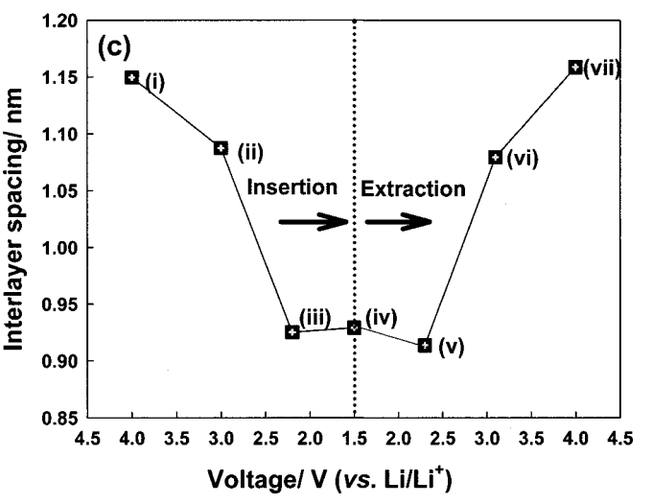

Figure 7. (a) The differential charging (Li^+ extraction) and discharging (Li^+ insertion) capacity plots (dQ/dV *vs.* V) for VO-8. The voltages where XRD analysis was made are indicated. (b) XRD profiles taken with cycling. Note the evolution of position, intensity, and broadness of (001) diffraction peaks with cycling. (c) The evolution of interlayer spacing with cycling. Note the mirror image between the insertion and extraction process.

Fig. 7a, the differential charging (Li^+ extraction) and discharging (Li^+ insertion) profiles of VO-8 are displayed with the voltage where the XRD analysis was made being indicated. The evolution of XRD profiles upon charge/discharge cycling is presented in Fig. 7b. A careful inspection on the (001) diffraction region at 5-12° reveals at least three apparent features. First, the (001) peak intensity shows a sharp decrease across 2.5 V during insertion, but a sharp recovery across 2.5 V in the extraction period. When Li^+ ions are inserted in the interlayer, the (001) diffraction peak becomes broader and weak due to the nonuniform layer spacing value. A sharp change in this diffraction intensity across 2.5 V illustrates the Li^+ insertion/extraction in/from the quasi-ordered layer stacking region at this potential range. Second, the peak position moves to the higher angle upon Li^+ insertion, then returns to the original position in the Li^+ extraction process. Third, the profile taken after one cycle looks identical to the initial one, indicative of no structural change during the charge/discharge cycling.

To gain a better insight into the second feature, the evolution of interlayer spacing with charge/discharge cycling is displayed separately in Fig. 7c. The fresh VO-8 electrode material shows an interlayer spacing of 1.15 nm. Upon lithiation down to 1.5 V, the layer spacing decreases in the range of 4.0 to 2.3 V, but stays at the same value in the range of 2.3 to 1.5 V. The shortening of interlayer spacing with lithiation is a result of a shielding effect that Li^+ ions exert on the negative charge residing on the apical oxides of VO_5 pyramids. Such an effect reduces the electrostatic repulsion force that acts between two adjacent V_2O_5 layers and leads to a shrinkage of the layer distance. The most prominent decrease in the layer spacing occurs from 3.0 to 2.3 V (that is, across 2.5 V), suggesting that Li^+ insertion mainly takes place near 2.5 V. The interlayer spacing is recovered to the original value upon Li^+ extraction with the same pattern. Here again, the most significant recovery in the interlayer spacing is observed across 2.5 V. The negligible change in the interlayer spacing at 2.3-1.5 V in both the insertion and extraction period indicates that Li^+ ions are not inserted/extracted in/from the interlayer at this voltage range. This observation indirectly supports our suggestion that Li^+ ions are inserted in an amorphous region when discharging across 1.7 V.

Conclusions

In this report, we provide a new preparation method for a-V_2O_5, and clarify the issue of electron/Li^+ imbalance and the nature of Li^+ storage sites. The following points are summarized.

1. a-V_2O_5 powders were synthesized by acidifying NH_4VO_3 solution. The degree of layer stacking became larger with an increase in the NH_4VO_3 concentration until an impurity phase ($NH_4V_3O_8 \cdot nH_2O$) developed. The sample prepared with 0.2 M NH_4VO_3 gave the highest degree of layer stacking. The surface area could be raised by drying the precipitate after replacing the pore water with solvents of a smaller surface tension.

2. The XANES spectra indicated that a-V_2O_5 reversibly reacts with Li^+ ions, and the vanadium oxidation state decreases to V(III) when discharged at $Li^+/V_2O_5 > 2.0$.

3. Three separable peaks appeared at 1.7, 2.5, and 2.9 V in the differential capacity plots (dQ/dV *vs.* V) for all the samples. The intensity of the 1.7 V peak was strongly correlated with the surface area of electrode materials, illustrating that Li^+ ions are inserted in amorphous region at this potential. It was also found that the peak intensity at 2.5 V is correlated with the intensity of (001) diffraction in XRD profiles. This finding suggests that Li^+ ions are inserted into the quasi-ordered interlayer stacking region near 2.5 V. This was further supported by XRD analysis, whereby a sharp decrease in both the intensity of (001) diffraction line and layer spacing was observed across 2.5 V.

4. The Li^+ insertion/extraction process was reversible as evidenced by the XANES and XRD results. The XANES spectrum taken after a charge/discharge cycling looked identical to the original one. Furthermore, the peak intensity of (001) diffraction line and the interlayer spacing value were fully recovered to the initial ones even after a cycling.

Acknowledgment

This work was supported by KOSEF via the Research Center for Energy Conversion and Storage, and also by the Ministry of Information and Communication in Korea (2002-5-013). The authors are grateful to authorities at the Pohang Light Source for X-ray absorption spectroscopic measurement.

References

1. J. Harreld, H. P. Wong, B. C. Dave, B. Dunn, and L. E. Nazar, *J. Non-Cryst. Solids*, **225**, 319 (1998).
2. H. Hirashima and K. Sudoh, *J. Non-Cryst. Solids*, **145**, 51 (1992).
3. F. Chaput, B. Dunn, P. Fugua, and K. Salloux, *J. Non-Cryst. Solids*, **188**, 11 (1995).
4. J. H. Harreld, B. Dunn, and L. F. Nazar, *Int. J. Inorg. Mater.*, **1**, 135 (1999).
5. S. D. Desai and E. L. Cussler, *Langmuir*, **14**, 277 (1998).
6. S. Bach, J. P. Pereira-Ramos, N. Baffier, and R. Messina, *J. Electrochem. Soc.*, **137**, 1042 (1990).
7. J. Livage, *Coord. Chem. Rev.*, **178-180**, 999 (1998).
8. H. K. Park, W. H. Smyrl, and M. D. Ward, *J. Electrochem. Soc.*, **142**, 1068 (1995).
9. H. K. Park and W. H. Smyrl, *J. Electrochem. Soc.*, **141**, L25 (1994).
10. A. L. Tipton, S. Passerini, B. B. Owens, and W. H. Smyrl, *J. Electrochem. Soc.*, **143**, 3473 (1996).
11. J. Livage, *Chem. Mater.*, **3**, 578 (1991).
12. D. B. Le, S. Passerini, A. L. Tipton, B. B. Owens, and W. H. Smyrl, *J. Electrochem. Soc.*, **142**, L102 (1995).
13. J. H. Harreld, W. Dong, and B. Dunn, *Mater. Res. Bull.*, **33**, 561 (1998).
14. W. Dong, D. R. Rolison, and B. Dunn, *Electrochem. Solid-State Lett.*, **3**, 457 (2000).
15. D. B. Le, S. Passerini, J. Guo, J. Ressler, B. B. Owens, and W. H. Smyrl, *J. Electrochem. Soc.*, **143**, 2099 (1996).
16. H. P. Wong, B. C. Dave, F. Leroux, J. Harreld, B. Dunn, and L. F. Nazar, *J. Mater. Chem.*, **8**, 1019 (1998).
17. D. B. Le, S. Passerini, F. Coustier, J. Guo, T. Soderstrom, B. B. Owens, and W. H. Smyrl, *Chem. Mater.*, **10**, 682 (1998).
18. S. Passerini, D. B. Le, W. H. Smyrl, M. Berrettoni, R. Tossici, R. Marassi, and M. Giorgetti, *Solid State Ionics*, **104**, 195 (1997).
19. K. Salloux, F. Chaput, H. P. Wong, B. Dunn, and M. W. Breiter, *J. Electrochem. Soc.*, **142**, L191 (1995).
20. D. R. Rolison and B. Dunn, *J. Mater. Chem.*, **11**, 963 (2001).
21. M. Giorgetti, S. Passerini, W. H. Smyrl, S. Mukerjee, X. Q. Yang, and J. McBreen, *J. Electrochem. Soc.*, **146**, 2387 (1999).
22. P. Ruetschi, *J. Electrochem. Soc.*, **131**, 2737 (1984).
23. P. Ruetschi, *J. Electrochem. Soc.*, **135**, 2657 (1988).
24. P. Ruetschi and R. Giovanoli, *J. Electrochem. Soc.*, **135**, 2663 (1988).
25. A. N. Mansour, P. H. Smith, W. M. Baker, M. Balasubramanian, and J. McBreen, *Electrochim. Acta*, **47**, 3151 (2002).
26. Y. J. Liu, J. L. Schindler, D. C. DeGroot, C. R. Kannewurf, and W. Hirpo, *Chem. Mater.*, **8**, 525 (1996).
27. S. Passerini, W. H. Smyrl, M. Berrettoni, R. Tossici, M. Rosolen, R. Marassi, and Decker, *Solid State Ionics*, **90**, 5 (1996).
28. C. G. Wu, D. C. DeGroot, H. O. Marcy, J. L. Schindler, C. R. Kannewurf, Y. J. Liu, W. Hirpo, and M. G. Kanatzidis, *Chem. Mater.*, **8**, 1992 (1996).
29. M. Tamura, M. Kurata, and H. Odani, *Bull. Chem. Soc. Jpn.*, **28**, 83 (1955).
30. P. Aldebert, N. Baffier, N. Gharbi, and J. Livage, *Mater. Res. Bull.*, **16**, 669 (1981).
31. O. Pelletier, P. Davidson, C. Bourgaux, C. Coulon, S. Regnault, and J. Livage, *Langmuir*, **16**, 5295 (2000).
32. F. Coustier, J. Hill, B. B. Owens, S. Passerini, and W. H. Smyrl, *J. Electrochem. Soc.*, **146**, 1355 (1999).
33. M. Giorgetti, S. Mukerjee, S. Passerini, J. McBreen, and W. H. Smyrl, *J. Electrochem. Soc.*, **148**, A768 (2001).
34. E. Potiron, A. Le Gal La Salle, A. Verbaere, Y. Piffard, and D. Guyomard, *Electrochim. Acta*, **45**, 197 (1999).